

Three-dimensional flux states as a model for the pseudogap phase of transition metal oxides

D. F. Schroeter* and S. Doniach

Department of Physics, Stanford University, Stanford, CA 94305

(Dated: March 22, 2022)

We propose that the pseudogap state observed in the transition metal oxides can be explained by a three-dimensional flux state, which exhibits spontaneously generated currents in its ground state due to electron-electron correlations. We compare the energy of the flux state to other classes of mean field states, and find that it is stabilized over a wide range of t and δ . The signature of the state will be peaks in the neutron diffraction spectra, the location and intensity of which are presented. The dependence of the pseudogap in the optical conductivity is calculated based on the parameters in the model.

PACS numbers: 71.10.Fd, 71.30.+h, 75.10.Lp

The motivation for this work is the observation of a pseudogap that opens up in optical conductivity measurements of the three-dimensional transition metal oxide SrRuO₃ [1] above its ferromagnetic transition temperature of $T_C \approx 150$ K. A pseudogap has also recently been seen in BaRuO₃ [2]. In this pseudogapped regime, $\rho(T)$ increases linearly with temperature, passing through the Ioffe-Regel limit without saturation [3], behavior indicative of a “bad metal” [4]. The optical conductivity in this state is proportional to the non-Fermi liquid behavior of $\omega^{-1/2}$ at high frequency and has a peak at low frequencies [1] at approximately 250 cm^{-1} , the precise location of the peak being temperature dependent.

We propose that this pseudogap state can be understood by considering a ground state with spontaneously generated electronic currents circulating around the plaquettes. The currents arise from electron-electron correlations, due to the bi-quadratic terms in the Hamiltonian. The state which we propose is a generalization of the two-dimensional flux states invented by Affleck and Marston [5], and studied in their chiral extension by Wen, Wilczek, and Zee [6]. Unlike the two-dimensional case, there is no possibility of fractional statistics in three dimensions. However, the spontaneous generation of gauge fields is a possibility in three dimensions, and these gauge fields can lead to a ground state with circulating electronic currents. Earlier work was done on three-dimensional flux states by Laughlin and coworkers [7, 8] and Zee [9].

In actuality, SrRuO₃ has 5 bands crossing the Fermi surface formed by hybridizing the Ruthenium d orbitals with the Oxygen p orbitals [10]. The crystal structure is orthorhombic, becoming cubic at temperatures greater than 900 K [11]. Undoubtedly, the actual electronic structure of SrRuO₃, and particularly the presence of a van Hove singularity near the Fermi surface, influence the material’s behavior. The model which we consider is vastly simplified and serves as a starting point for consid-

ering the nature of the pseudogapped state in the three-dimensional transition metal oxides. A model which incorporates some of these electronic features, but does not focus on the pseudogap regime, has been proposed by Laad and Müller-Hartmann [12].

I. MODEL SYSTEM

The Hamiltonian that we consider is the single orbital t - J model given by

$$H = J \sum_{\langle ij \rangle} \mathbf{S}_i \cdot \mathbf{S}_j - t \sum_{\langle ij \rangle \sigma} c_{i\sigma}^\dagger c_{j\sigma}, \quad (1)$$

where the sum over $\langle ij \rangle$ denotes nearest neighbors on a cubic three-dimensional lattice. Implicit in this equation is that we have set $U = \infty$. The hopping matrix element t which appears in Equation 1 is taken to be an effective hopping element, which has been greatly reduced due to this on-site Coulomb repulsion. The value of t will be set by two calculations in this paper: the stability of the flux phase versus other mean field states calculated in Section II, and the value of the optical conductivity calculated in Section V.

The spin operators may be written in terms of the fermion operators to give the Hamiltonian

$$H = -\frac{J}{2} \sum_{\langle ij \rangle} \sum_{\sigma \sigma'} c_{i\sigma}^\dagger c_{j\sigma} c_{j\sigma'}^\dagger c_{i\sigma'} - t \sum_{\langle ij \rangle} \sum_{\sigma} c_{i\sigma}^\dagger c_{j\sigma} + \frac{3NJ}{4}. \quad (2)$$

The Hamiltonian will be treated in the mean field, or Hartree-Fock approximation. We make the replacement:

$$\sum_{\sigma} c_{i\sigma}^\dagger c_{j\sigma} \rightarrow \chi_{ij} + \left(\sum_{\sigma} c_{i\sigma}^\dagger c_{j\sigma} - \chi_{ij} \right) \quad (3)$$

The assumption is made that the term in brackets, which corresponds to fluctuations about the mean-field χ_{ij} , is small and can be included only to linear order. The re-

*Electronic address: dfs@Stanford.edu

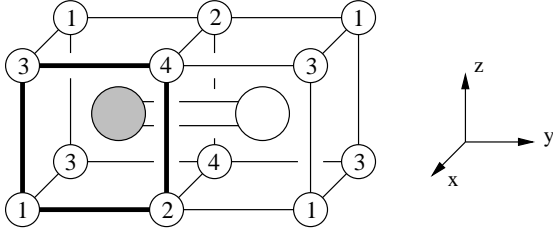


FIG. 1: Unit cell for symmetry-broken bond Hamiltonian. The dark line passes through the four atoms in the planar unit cell. The spheres at the center of the cubes represent oppositely charged Dirac monopoles with the “tail” running through the interface between the two cubes.

sulting Hamiltonian is given by

$$H = \frac{J}{2} \sum_{\langle ij \rangle} \left\{ |\chi_{ij}|^2 - 2 \left[\left(\chi_{ij} + \frac{t}{J} \right) c_j^\dagger c_i + \text{H.c.} \right] \right\}, \quad (4)$$

where we have dropped the redundant spin index. There is no a priori reason to believe that the fluctuations about the mean field will be small, although it has been rigorously shown in the two-dimensional case for the large n limit [5], where n is the particle spin.

We allow the χ_{ij} to break the translational symmetry of the lattice. We choose a four-atom unit cell as shown in Figure 1. The lattice is generated by the primitive translation vectors $(1, 0, 1)$, $(1, 0, -1)$, and $(0, 2, 0)$, in units of the bondlength b . The χ_{ij} in Equation 4 are then parameterized by 12 complex numbers. We use the notation $\chi_{i\nu}$, where the index $i = 1, \dots, 4$ is the location of the atom in the unit cell and the index ν gives the direction $\{x, y, z\}$.

This choice is made because it allows for the formation of a π -per plaquette flux phase, something that a two atom unit cell does not allow in three dimensions. The model is computationally simpler than the eight-band model studied by Laughlin [7, 8], at the expense of picking out a preferred direction. To get a feel for what this corresponds to, one can think of the gauge fields in the sample as being generated by Dirac monopoles of alternating charge sitting at the centers of each cube. The “tails” of the monopoles are connected to form dipoles. The \hat{y} direction in our model corresponds to the dipolar axis.

The self-consistency of the model is the requirement that the energy as determined by Equation 4 be a local minimum with respect to variations of the twelve complex parameters $\chi_{i\nu}$. This can be seen by writing

$$\langle H \rangle = \frac{\mathcal{N}J}{8} \sum_{i=1}^4 \sum_{\nu=1}^3 \left\{ |\chi_{i\nu}|^2 - 2 \left[\left(\chi_{i\nu}^* + \frac{t}{J} \right) \langle c_i^\dagger c_{i+\nu} \rangle + \text{H.c.} \right] \right\}. \quad (5)$$

Minimizing this function with respect to $\chi_{i\nu}^*$ gives the

self-consistency relation

$$\langle c_i^\dagger c_{i+\nu} \rangle = \frac{\chi_{i\nu}}{2}. \quad (6)$$

Note also that at this minimum, the expectation value of the Hamiltonian is given by

$$\langle H \rangle = -\frac{\mathcal{N}J}{8} \sum_{i=1}^4 \sum_{\nu=1}^3 \left[|\chi_{i\nu}|^2 + 2\frac{t}{J} \text{Re}(\chi_{i\nu}) \right]. \quad (7)$$

The Hamiltonian in Equation 4 contains both a field strength and a term which we define as the bond Hamiltonian:

$$H_B = J \sum_{\langle ij \rangle} \sum_{\sigma} \left(\chi_{ji} + \frac{t}{J} \right) c_{i\sigma}^\dagger c_{j\sigma} + \text{H.c.} \quad (8)$$

The bond Hamiltonian can be diagonalized by introducing a set of operators

$$\psi_{\mathbf{q}\lambda}^\dagger = \frac{1}{\sqrt{\mathcal{N}}} \sum_{\ell} e^{i\mathbf{q} \cdot \mathbf{r}_\ell} u_{\mathbf{q}\lambda}(\ell) c_{\mathbf{r}_\ell}^\dagger, \quad (9)$$

where \mathcal{N} is the number of sites in the lattice, λ is the band index which runs from 1 to 4 and the $u_{\mathbf{q}\lambda}(\ell)$ are a set of functions periodic in the unit cell. The bands are determined by the eigenvalue equation

$$H_{\mathbf{q}} u_{\mathbf{q}\lambda} = \epsilon_{\mathbf{q}\lambda} u_{\mathbf{q}\lambda}, \quad (10)$$

where $H_{\mathbf{q}}$ is written in terms of the hopping elements and $u_{\mathbf{q}\lambda}$ is a 4 component vector $u_{\mathbf{q}\lambda}(1) \cdots u_{\mathbf{q}\lambda}(4)$. For the unit cell depicted in Figure 1, the Hamiltonian takes the form

$$H_{\mathbf{q}} = J \begin{pmatrix} 0 & \eta_1 & \eta_3 & 0 \\ \eta_1^* & 0 & 0 & \eta_4 \\ \eta_3^* & 0 & 0 & \eta_2 \\ 0 & \eta_4^* & \eta_2^* & 0 \end{pmatrix}, \quad (11)$$

where

$$\begin{aligned} \eta_1 &= \tilde{\chi}_{1y} e^{iq_y} + \tilde{\chi}_{2y}^* e^{-iq_y} \\ \eta_2 &= \tilde{\chi}_{3y} e^{iq_y} + \tilde{\chi}_{4y}^* e^{-iq_y} \\ \eta_3 &= \tilde{\chi}_{1x} e^{iq_x} + \tilde{\chi}_{1z} e^{iq_z} + \tilde{\chi}_{3x}^* e^{-iq_x} + \tilde{\chi}_{3z}^* e^{-iq_z} \\ \eta_4 &= \tilde{\chi}_{2x} e^{iq_x} + \tilde{\chi}_{2z} e^{iq_z} + \tilde{\chi}_{4x}^* e^{-iq_x} + \tilde{\chi}_{4z}^* e^{-iq_z}. \end{aligned} \quad (12)$$

The tilde in the expression above means that these numbers include the actual hopping element: $\tilde{\chi}_{i\nu} = \chi_{i\nu} + t/J$. The eigenenergies for the four bands are given by

$$\epsilon_{\mathbf{q}} = \pm J \sqrt{\frac{\eta_i \eta_i^*}{2} \pm \sqrt{\left(\frac{\eta_i \eta_i^*}{2} \right)^2 - |\eta_1 \eta_2^* - \eta_3 \eta_4^*|^2}}, \quad (13)$$

with the usual Einstein summation convention. In Section III we will consider the band structure and eigenstates of one particular solution of the bond Hamiltonian,

the flux state where the hopping elements are complex and equal in magnitude: $|\chi_{i\nu}| = \chi$ for all i, ν .

For $t = 0$ the gauge fields χ_{ij} are unobservable. However, as soon as t is increased they lead to real circulating electronic currents. Consider the site i and the six sites j which are its nearest neighbors. The sum of the currents flowing outward from site i is then the time rate of change of the number operator n_i on site i

$$\begin{aligned} \sum_j \dot{n}_i &= \left\langle \frac{\partial}{\partial t} n_i \right\rangle = \frac{i}{\hbar} \langle [H_B, n_i] \rangle, \\ &= \frac{2i}{\hbar} \sum_j (J\chi_{ij} + t) \langle c_j^\dagger c_i \rangle - \text{H.c.}, \end{aligned} \quad (14)$$

where the factor of 2 arises from the spin. The term $\chi_{ij} \langle c_j^\dagger c_i \rangle$ is real and gives no contribution, but for $t > 0$ and χ_{ij} complex, the bonds carry electronic currents. These currents are the signature of the flux state. They have long-range order and can be probed by neutron diffraction as will be shown in Section IV.

II. THE PHASE DIAGRAM

The Hamiltonian described in Section I admits a number of self-consistent solutions. We have performed a numerical search as a function of the hopping element t and the doping δ . The function to be minimized is

$$E = \frac{\mathcal{N}}{8} \left[J \sum_{i\nu} |\chi_{i\nu}|^2 + 2 \frac{1}{\mathcal{N}_m} \sum_{\mathbf{k}\lambda} \epsilon_{\mathbf{k}\lambda} \right], \quad (15)$$

where $\mathcal{N}_m = \mathcal{N}/4$ is the number of unit cells in the lattice. The search is performed using Powell's method in the space of the $\chi_{i\nu}$. At each point in the space, the bands are determined by Equation 13, and the lower magnetic bands are filled up with $N_e = \mathcal{N}(1 - \delta)$ electrons.

Our search is limited to three classes of states. We consider the flux phase with $|\chi_i| = |\chi|$ for all i with the phases of the hopping elements unconstrained. At $t = \delta = 0$ the flux phase has flux $\Phi = \pi$ per plaquette as defined by

$$e^{i\Phi} = \prod_{\text{plaquette}} \frac{\tilde{\chi}_{i\nu}}{|\tilde{\chi}_{i\nu}|}. \quad (16)$$

Note that a flux of π and a flux of $-\pi$ per plaquette are indistinguishable since in either case the electron acquires a phase of -1 upon traversing the plaquette. This is the chiral symmetry of the model. Away from $t = \delta = 0$, the flux per plaquette is no longer π and the chiral symmetry is broken.

Another state that we have considered is the dimer state. In this case each site forms a bond with a neighboring site. In the case of $t = \delta = 0$, one particular manifestation of the state is $\chi_{1z} = \chi_{4x} = 1$ with all other $\chi_{i\nu} = 0$. The dimer state has flat bands $\epsilon_q = \pm J$ and can

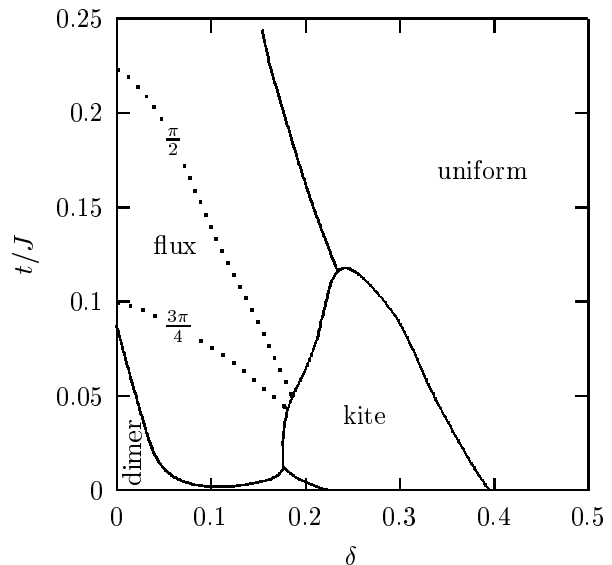


FIG. 2: Phase Diagram for Bond States. The diagram shows the competition between the four types of states considered in the text. The contours in the flux phase region show the average flux per plaquette, as defined by Equation 16.

be considered to be a charge-density state with the charge localized on the bonds for which $\chi_{i\nu} = 1$ [5]. Away from the point $t = \delta = 0$, the state becomes partially dimerized. There are in principle a number of non-equivalent dimer solutions, but the solution mentioned above appears to be the lowest energy configuration.

At values of $\delta \gtrsim 0.2$ another local minimum is the kite state which has $\chi_{1y} = \chi_{2x} = \chi_{3z} = \chi_{4y} \neq \chi_{i\nu}$. The state is called a kite state because the lines of charge, if the analogy from the dimer state above is used, form zigzagging patterns through the lattice, and could lead to a lattice distortion from the large Coulomb repulsion between charged lines. This particular instantiation of the kite state is chosen for the same reasons as the dimer above. The last state which is considered is the uniform state with all $\chi_{i\nu}$ equal and real valued. This state is a simple Fermi liquid, with a renormalized value of the hopping matrix element.

The phase diagram is shown in Figure 2. While we have performed the calculation for an arbitrary flux state as described above, the phase diagram shows a calculation performed using a restricted parameter set. The parameters used are shown as different arrows in Figure 3 below. This is done because at $\delta \approx 0.1$, there is a transition to a flux phase with a different type of ordering which is outside the scope of the current discussion. Apart from this transition, there is no qualitative change in the phase diagram when the unconstrained flux state is considered. From the phase diagram we see that the flux state is stabilized over a fairly wide range of doping, but that the flux per plaquette decreases from the value of π as one leaves the point $t = \delta = 0$. In the calculations which follow we will assume that $t/J = 0.1$,

a point at which the highly symmetric π -per plaquette flux state discussed below in Section III is a reasonable approximation to the actual mean field state.

One must also consider the possibilities of other types of order which are not described by the mean-field χ_{ij} . The most insidious of these is antiferromagnetic order. At $t = \delta = 0$, the energies of the two stabilized states discussed above are

$$E_{\text{dimer}} = -\frac{\mathcal{N}J}{4}, \quad E_{\text{flux}} \approx -0.95 \frac{\mathcal{N}J}{4}. \quad (17)$$

For comparison, the Néel state, which is characterized by

$$\chi_{ij} = 0 \quad \left\langle c_{i\sigma}^\dagger \sigma^z c_{i\sigma'} \right\rangle = (-1)^i, \quad (18)$$

has an energy of $-3\mathcal{N}J/4$, lower than either of the two bond states at $t = \delta = 0$. In order for the bond states to be actualized, a term has to be added which will destabilize the antiferromagnetic order. This can be done by adding a next-nearest neighbor hopping term J' [13], in which case the energy of the Néel state will be

$$E_{\text{Néel}} = -\frac{3\mathcal{N}J}{4} \left(1 - 2\frac{J'}{J} \right). \quad (19)$$

The energies of the bond states are actually unchanged up to a value of $J'/J \approx 1/3$, which is the threshold for acquiring a nonzero value of the next nearest neighbor χ_{ij} as shown by Laughlin and Zou [14]. At the value $J' = J/3$, the energy of the Néel state is equal to the energy of the dimer state and very close to the energy of the flux state. Doping will also serve to destabilize the antiferromagnet so that the crossover will actually occur at a lower value of J' than the one reported here. Therefore, while it is not treated explicitly in this paper, some term such as the next-nearest neighbor J' must be added to this model in order to make the bond states energetically favorable with respect to the Néel ordered state.

III. THE FLUX PHASE

In the calculations which follow, we consider the π per plaquette flux phase described in Section II which is only truly stabilized at $\delta = t = 0$. Some care must be used in selecting this state since at $t = \delta = 0$ the system is invariant under a gauge transformation where

$$c_i \rightarrow e^{i\phi_i} c_i, \quad \chi_{ij} \rightarrow e^{i(\phi_j - \phi_i)} \chi_{ij}. \quad (20)$$

Away from this point, this symmetry disappears, and the low-energy state is the one for which the quantity

$$\sum_{i\nu} \text{Re} [\chi_{i\nu}], \quad (21)$$

is a maximum as can be seen from Equation 7. The state is shown in Figure 3. It can be found by either maximizing the function in Equation 21 for an arbitrary gauge

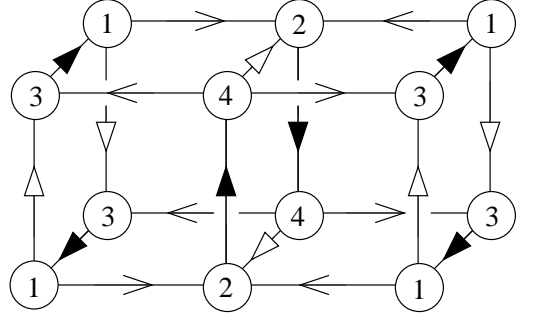


FIG. 3: The π per plaquette flux phase. All bonds have the same magnitude. The arrows correspond to complex phases of ϕ ($>$), $\phi - \pi/4$ (\triangleright), and $3\pi/4 - \phi$ (\blacktriangleright), where ϕ is determined by $\tan \phi = \sqrt{2}$. This diagram shows the same portion of the lattice as is shown in Figure 1.

transformation, or by numerically continuing a state from $t > 0$ down to $t = 0$. The choice of the correct symmetry-breaking gauge is important since it will affect the distribution of electronic currents in the sample and hence observable features such as the neutron diffraction and optical conductivity.

In this state, the Hamiltonian in Equation 9 can be rewritten using a set of Dirac matrices α_x , α_y , and α_z such that

$$H_{\mathbf{q}} = 2J|\chi| \sum_{\nu} \cos(q_{\nu}b) \alpha_{\nu}, \quad (22)$$

where the matrices satisfy the algebra

$$\{\alpha_i, \alpha_j\} = 2\delta_{ij}. \quad (23)$$

Explicit forms for the matrices are given in Appendix. It is found numerically that $|\chi| \approx 0.4$. The eigenvalues of the Hamiltonian are twofold degenerate and are given by

$$\epsilon_{\mathbf{q}} = \pm 2J|\chi| \sqrt{\sum_{\nu} \cos^2(q_{\nu}b)}. \quad (24)$$

The band structure is shown in Figure 4. At half-filling the Fermi surface reduces to two isolated points at $\mathbf{qb} = (\pi/2, \pi/2, \pi/2)$ and $\mathbf{qb} = (\pi/2, \pi/2, -\pi/2)$ shown at the point Σ in Figure 4. The low energy excitations about these points are relativistic.

In order to calculate the neutron cross-section and the optical conductivity, we also will need the eigenvectors which appear in Equation 9. The matrix \mathbf{u} whose rows correspond to the bands 1...4 and whose columns correspond to the position in the unit cell is given by

$$\mathbf{u}_{\mathbf{q}} = \frac{1}{\sqrt{2}} \begin{pmatrix} |\eta_{\mathbf{q}}| & -\frac{\eta_{\mathbf{q}}}{|\eta_{\mathbf{q}}|} e^{-i\phi} & 0 & \frac{\eta_{\mathbf{q}}}{|\eta_{\mathbf{q}}|} \gamma_{\mathbf{q}} \\ |\gamma_{\mathbf{q}}| & 0 & \frac{\gamma_{\mathbf{q}}}{|\gamma_{\mathbf{q}}|} e^{-i\phi} & -\eta_{\mathbf{q}} \frac{\gamma_{\mathbf{q}}}{|\gamma_{\mathbf{q}}|} \\ |\eta_{\mathbf{q}}| & \frac{\eta_{\mathbf{q}}}{|\eta_{\mathbf{q}}|} e^{-i\phi} & 0 & -\gamma_{\mathbf{q}} \frac{\eta_{\mathbf{q}}}{|\eta_{\mathbf{q}}|} \\ |\gamma_{\mathbf{q}}| & 0 & -\frac{\gamma_{\mathbf{q}}}{|\gamma_{\mathbf{q}}|} e^{-i\phi} & -\eta_{\mathbf{q}} \frac{\gamma_{\mathbf{q}}}{|\gamma_{\mathbf{q}}|} \end{pmatrix}, \quad (25)$$

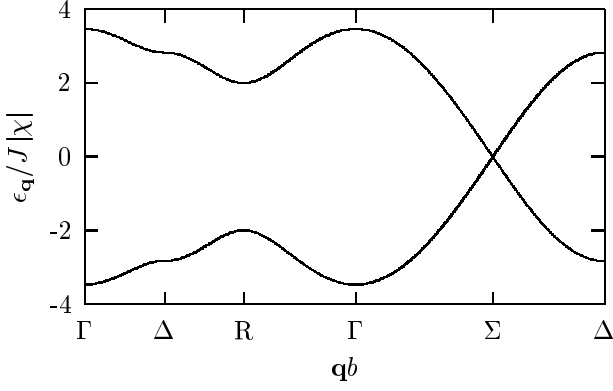


FIG. 4: Flux Phase band structure. Points in the Brillouin zone are $\Gamma = (0, 0, 0)$, $\Delta = (\pi/2, 0, 0)$, $R = (\pi/2, 0, \pi/2)$, and $\Sigma = (\pi/2, \pi/2, \pi/2)$. There are two distinct Dirac points located at $\mathbf{qb} = (\pi/2, \pi/2, \pi/2)$ and $\mathbf{qb} = (\pi/2, \pi/2, -\pi/2)$.

where we have defined the quantities

$$\eta_{\mathbf{q}} = \frac{\cos q_y b}{\Gamma_{\mathbf{q}}} \quad \gamma_{\mathbf{q}} = e^{-i\frac{\pi}{4}} \frac{\cos q_x b - i \cos q_z b}{\Gamma_{\mathbf{q}}} \quad \Gamma_{\mathbf{q}} = \sqrt{\sum_{\nu} \cos^2(q_{\nu} b)}. \quad (26)$$

The phases of the eigenvectors in Equation 25 have been selected so that the eigenstates in Equation 9 are invariant under $\mathbf{q} \rightarrow \mathbf{q} + \mathbf{Q}$ where \mathbf{Q} is any vector in the reciprocal lattice.

IV. NEUTRON SCATTERING

The flux states can be probed by neutron scattering, as the neutron spin interacts with the magnetic dipoles generated by the real electron currents circulating on the plaquettes. The interaction potential [15] is written

$$V(\mathbf{r}) = 2 \sum_{\langle ij \rangle} t \left(c_i^{\dagger} c_j - \text{H.c.} \right) \exp \left[\frac{ie}{\hbar c} \int_{\mathbf{x}_i}^{\mathbf{x}_j} \mathbf{A} \cdot d\ell \right], \quad (27)$$

where the vector potential is given by

$$\mathbf{A} = \boldsymbol{\mu} \times \frac{\mathbf{r}_e - \mathbf{r}_n}{|\mathbf{r}_e - \mathbf{r}_n|^3}, \quad \boldsymbol{\mu} = -\gamma \frac{e\hbar}{m_n c} \mathbf{S}. \quad (28)$$

In these expressions \mathbf{S} is the neutron spin and $\gamma \approx 1.91$ is a constant. It can be shown [17] that

$$\int d\mathbf{r} e^{i\mathbf{q} \cdot \mathbf{r}_n} V(\mathbf{r}) = i(\gamma r_0) \left(\frac{m}{m^*} \right) \frac{8\pi\hbar^2}{m_n} \times \frac{1}{|\mathbf{qb}|^2} \sum_{\nu} J_{\nu} \frac{\hat{\nu} \cdot (\mathbf{S} \times \mathbf{q})}{\mathbf{q} \cdot \hat{\nu}}, \quad (29)$$

with the current operator defined as

$$J_{\nu} = \sum_{\mathbf{k}} c_{\mathbf{k}+\mathbf{q}}^{\dagger} c_{\mathbf{k}} f_{\nu}(\mathbf{k}, \mathbf{q}) \quad f_{\nu}(\mathbf{k}, \mathbf{q}) = \cos(k_{\nu} b) - \cos(k_{\nu} b + q_{\nu} b). \quad (30)$$

In these expressions we have replaced the hopping element t by $\hbar^2/2m^*b^2$, with m^* the effective mass. Since we are assuming (see Section II) that $t/J = 0.1$, the effective mass will be quite large. If we assume that J takes the typical value of 0.1 eV, we have $m^* \approx 15m$. The vector $\hat{\nu}$ is a unit vector with the sum running over the x , y , and z directions.

Converting this to a cross-section and averaging over the spin, assuming that the incoming beam is unpolarized, the expression for the cross-section is given by

$$\frac{d\sigma}{d\Omega} = (\gamma r_0)^2 \left(\frac{m}{m^*} \right)^2 \frac{4}{|\mathbf{qb}|^4} \sum_{\nu < \nu'} \left| \frac{q_{\nu}}{q_{\nu'}} \langle J_{\nu'} \rangle - \frac{q_{\nu'}}{q_{\nu}} \langle J_{\nu} \rangle \right|^2. \quad (31)$$

In order to calculate the matrix elements in Equation 31, we need to rewrite the current operator in terms of the eigenstates of our system. We first break up the momentum sum so that it runs only over the first Brillouin zone

$$J_{\nu} = \sum_{\mathbf{k}} \sum_{i=1}^4 c_{\mathbf{k}+\mathbf{q}+\mathbf{Q}_i}^{\dagger} c_{\mathbf{k}+\mathbf{Q}_i} f_{\nu}(\mathbf{k} + \mathbf{Q}_i, \mathbf{q}), \quad (32)$$

where $\mathbf{Q}_1 b = \mathbf{0}$, $\mathbf{Q}_2 b = (\pi, 0, \pi)$, $\mathbf{Q}_3 b = (0, \pi, 0)$, and $\mathbf{Q}_4 b = \boldsymbol{\pi}$. We can rewrite the electron operators at momentum $\mathbf{k} + \mathbf{Q}$ in terms of the $c_{\mathbf{q}}(\ell)$ defined as

$$c_{\mathbf{q}}^{\dagger}(\ell) = \frac{1}{\sqrt{N_m}} \sum_{\mathbf{R}} e^{i\mathbf{q} \cdot (\mathbf{R} + \mathbf{r}_{\ell})} c_{\mathbf{R} + \mathbf{r}_{\ell}}^{\dagger}, \quad (33)$$

where \mathbf{R} runs over all the unit cells and \mathbf{r}_{ℓ} is the position of the ℓ^{th} atom in the unit cell. This introduces a matrix g with elements $g_{i\ell} = \exp[i\mathbf{Q}_i \cdot \mathbf{r}_{\ell}]/2$, and results in the current operator

$$J_{\nu} = \sum_{\mathbf{k}} \sum_{imp} g_{im} g_{ip} c_{\mathbf{k}+\mathbf{q}}^{\dagger}(m) c_{\mathbf{k}}(p) f_{\nu}(\mathbf{k} + \mathbf{Q}_i, \mathbf{q}). \quad (34)$$

We also note that $f_{\nu}(\mathbf{k} + \mathbf{Q}_i, \mathbf{q}) = [\bar{Q}^{\nu}]_{ii} f_{\nu}(\mathbf{k}, \mathbf{q})$, where the matrix \bar{Q}^{ν} is diagonal with elements $\exp[i\mathbf{Q}_i \cdot \boldsymbol{\nu} b]$. The sum on i can then be performed to obtain

$$J_{\nu} = \sum_{\mathbf{k}} \sum_{mp} c_{\mathbf{k}+\mathbf{q}}^{\dagger}(m) [g\bar{Q}^{\nu}g]_{mp} c_{\mathbf{k}}(p) f_{\nu}(\mathbf{k}, \mathbf{q}). \quad (35)$$

The matrix $g\bar{Q}^{\nu}g$ in the above expression has a natural interpretation. It merely connects all sites in the lattice which are connected by a hopping element in the $\boldsymbol{\nu}$ direction. It can be written in the form

$$g\bar{Q}^{\nu}g = \begin{pmatrix} \sigma^x & 0 \\ 0 & \sigma^x \end{pmatrix} \delta_{\nu y} + \begin{pmatrix} 0 & \mathbb{1} \\ \mathbb{1} & 0 \end{pmatrix} (\delta_{\nu x} + \delta_{\nu z}). \quad (36)$$

Finally, we can rewrite Equation 35 by inverting the eigenvector matrix in Equation 25. This gives

$$J_{\nu} = \sum_{\mathbf{k}} \sum_{\lambda\lambda'} \left[u_{\mathbf{k}} (g\bar{Q}^{\nu}g) u_{\mathbf{k}+\mathbf{q}}^{\dagger} \right]_{\lambda\lambda'} f_{\nu}(\mathbf{k}, \mathbf{q}) \psi_{\lambda, \mathbf{k}+\mathbf{q}}^{\dagger} \psi_{\lambda', \mathbf{k}}. \quad (37)$$

If we assume that the lower bands are completely filled, we can then write a simple expression for the expectation values of these matrix elements.

$$\langle J_\nu \rangle = \sum_{\boldsymbol{\tau}} \sum_{\mathbf{k}}' \text{Tr}' \left[u_{\mathbf{k}} (g \bar{Q}^\nu g) u_{\mathbf{k}+\mathbf{q}}^\dagger \right] f_\nu(\mathbf{k}, \mathbf{q}) \delta_{\mathbf{q}\boldsymbol{\tau}} \quad (38)$$

The prime on the trace indicates that it runs only over the lower two bands, and the sum on $\boldsymbol{\tau}$ runs over all vectors in the reciprocal lattice.

Expression 38 is quite general and can be used to calculate properties away from zero doping by restricting the sum on \mathbf{k} such that $\mathbf{k} < \mathbf{k}_F$. Additionally, this equation assumes nothing about the actual structure of the eigenvector matrix $u_{\mathbf{k}}$. Specializing to the case of the flux state discussed in Section III, the trace for $\nu = y$ is

$$i \left(1 - \frac{\gamma_{\mathbf{k}+\mathbf{q}}^*}{\gamma_{\mathbf{k}}^*} \right) \eta_{\mathbf{k}} \sin \phi. \quad (39)$$

Here we have used the fact that $\eta_{\mathbf{k}+\mathbf{q}} = -\eta_{\mathbf{k}}$, a condition enforced by the presence of f_y in Equation 38. We see that the trace is zero unless $\gamma_{\mathbf{k}+\mathbf{q}} = -\gamma_{\mathbf{k}}$, which means that $\langle J_y \rangle$ vanishes unless $q_y b$ is an odd multiple of π for all ν . For the $\nu = x$ and $\nu = z$ cases, the traces are the same as can be seen from Equation 36. They are given by

$$i \left(1 - \frac{\eta_{\mathbf{k}+\mathbf{q}}}{\eta_{\mathbf{k}}} \right) \text{Im} \gamma_{\mathbf{k}} \cos \phi - i \left(1 + \frac{\eta_{\mathbf{k}+\mathbf{q}}}{\eta_{\mathbf{k}}} \right) \text{Re} \gamma_{\mathbf{k}} \sin \phi, \quad (40)$$

where we have taken $\gamma_{\mathbf{k}+\mathbf{q}} = -\gamma_{\mathbf{k}}$ for the same reasons as above. This expression takes two different values depending on whether $q_y b$ is an even or an odd multiple of π .

Scattering will only occur at the reciprocal lattice vectors, as guaranteed by the delta function in Equation 38. The reciprocal lattice is shown in Figure 5. There is no magnetic scattering at the nuclear locations, since they occur at even multiples of π . There is additionally no scattering at the line centers $\mathbf{qb} = \pi \hat{\mathbf{y}}$, since all three matrix elements vanish at these points. Scattering does occur at both the face-centers at $\mathbf{qb} = (\pi, 0, \pi)$ and at the body-center at $\mathbf{qb} = \boldsymbol{\pi}$. The former distinguishes the scattering from Bragg scattering from a cubic antiferromagnet. It is likely that the actual material would consist of domains containing all dipolar orientations, so that scattering would actually be observed at all the face-centers.

The magnitude of the scattering will in general be quite small. We write the cross section as

$$\frac{d\sigma}{d\Omega} = \mathcal{N}_m \frac{(2\pi)^3}{v_{0m}} (\gamma r_0)^2 \left(\frac{m}{m^*} \right)^2 \sum_{\boldsymbol{\tau}} M(\mathbf{q}) \delta(\mathbf{q} - \boldsymbol{\tau}), \quad (41)$$

where we have rewritten the Kronecker delta function from Equation 38 in terms of the Dirac delta function with the proper normalization of $(2\pi)^3/V$. The term $v_{0m} = 4b^3$ is the volume of the unit cell. The structure factor is given by

$$M(\mathbf{q}) = \frac{4}{3} \frac{|\chi|^2}{|\mathbf{qb}|^2} \left[(3 + \cos q_y b) \left(\frac{1}{(q_x b)^2} + \frac{1}{(q_z b)^2} \right) + 4 \frac{1 - \cos q_y b}{(q_y b)^2} \right] (1 - \cos q_x b) (1 - \cos q_z b). \quad (42)$$

In deriving this expression, we have repeatedly used the fact that

$$\frac{1}{\mathcal{N}_m} \sum_{\mathbf{k}}' \frac{\cos k_\nu \cos k_{\nu'}}{\Gamma_{\mathbf{k}}} = |\chi| \delta_{\nu\nu'}, \quad (43)$$

with the $\Gamma_{\mathbf{k}}$ defined as in Equation 26. This relation follows from the symmetry of the momentum sum and Equation 15. The structure factor in Equation 42 takes the same value at the two smallest scattering angles corresponding to the points $\mathbf{Q}_2 b = (\pi, 0, \pi)$ and $\mathbf{Q}_4 b = \boldsymbol{\pi}$ in the reciprocal lattice:

$$M(\mathbf{q}) = \frac{64}{3\pi^4} |\chi|^2 \quad (44)$$

To give a feel for the order of magnitude of the scattering from the flux states, we compare to the scattering from

an antiferromagnet. In that case one has

$$\left. \frac{d\sigma}{d\Omega} \right|_{AF} = \frac{2}{3} \mathcal{N}_m^{AF} \frac{(2\pi)^3}{v_{0m}^{AF}} (\gamma r_0)^2 \langle S^\eta \rangle^2 \sum_{\boldsymbol{\tau}} |F(\boldsymbol{\tau})|^2 \delta(\mathbf{q} - \boldsymbol{\tau}), \quad (45)$$

where the factor of $2/3$ arises by assuming that the sublattice magnetization is along a crystallographic axis. We can estimate the form factor for the antiferromagnet by assuming it is the same as that of chromium, a typical band antiferromagnet. Chromium has a form factor of $F(\boldsymbol{\pi}/b) \approx 0.4$ [16]. The unit cell in the flux phase is twice as large as the antiferromagnetic unit cell and therefore $\mathcal{N}_m^{AF} = 2\mathcal{N}_m$ and $v_{0m}^{AF} = v_{0m}/2$. Assuming that the spins are 50% polarized such that $\langle S^\eta \rangle = 1/4$, and taking $m^* = 15m$, we see that the scattering from the antiferromagnet is roughly 170 times larger than the scattering from the flux state at the wave-vector $\mathbf{qb} = \boldsymbol{\pi}$. Note that the discrepancy in size is due primarily to the

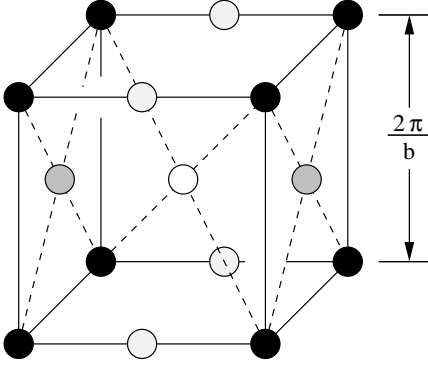


FIG. 5: Reciprocal Lattice Vectors for Flux Phase. The black dots show the scattering from the nuclear centers. The white dot shows the antiferromagnetic scattering vector at $\mathbf{qb} = \pi$. The shaded dots at the face centers show those points in the reciprocal lattice space of the flux phase which produce scattering, and the lighter shaded dots along the line centers show those points in the reciprocal lattice space which do not produce scattering.

size of the effective hopping element t , which must be small compared to J if the flux phase is going to be stabilized away from $\delta = 0$ as was shown in Section II.

V. OPTICAL CONDUCTIVITY

In our model, the peak in the optical conductivity arises from transitions between the bands shown in Figure 4. The model is too simple to accurately predict the optical conductivity of a material such as SrRuO_3 . However, the calculation illustrates both the dependence of the location of the peak on the spin-exchange energy J and the intensity of the peak on the ratio of t/J .

The calculation of the optical conductivity is very similar to that of the neutron diffraction. In this case we couple the system to a time-dependent vector potential $\mathbf{A} = A(t)\hat{\nu}$, where the vector potential's time dependence and relation to the electric field are given by

$$A(t) = Ae^{-i\omega t} \quad \mathbf{E} = \frac{i\omega}{c}\mathbf{A}. \quad (46)$$

We assume that the wavelength of the light is long enough that we can ignore any spatial dependence in the fields. The vector potential couples to the hopping terms in the Hamiltonian. A phase is acquired according to

$$c_j^\dagger c_i \rightarrow c_j^\dagger c_i \exp \left[\frac{ie}{\hbar c} \int_{\mathbf{x}_i}^{\mathbf{x}_j} \mathbf{A} \cdot d\boldsymbol{\ell} \right]. \quad (47)$$

It is important to note that the corresponding χ_{ij} appearing in Equation 4 also acquire an equal and opposite phase so that when we expand the Hamiltonian to linear order in the vector potential $A(t)$ we do not get any contribution from the terms proportional to χ_{ij} . The

perturbation to the Hamiltonian is

$$H' = -\frac{L}{c}\mathbf{A} \cdot \mathbf{j}, \quad (48)$$

where $L = \mathcal{N}^{1/3}b$ is the length of the sample and the current operator in the ν direction is given by

$$j_\nu = \frac{2iteb}{\hbar L} \sum_i \left[c_i^\dagger c_{i+\nu} - c_{i+\nu}^\dagger c_i \right]. \quad (49)$$

Note that the operator in Equation 49 defines the total current, not the current density, flowing in the ν direction. The complex optical conductivity is related to the induced current density in the sample by

$$\mathbf{J}_{\text{ind}} = \sigma \mathbf{E}. \quad (50)$$

The induced current can be calculated using linear response theory. In that case it can be shown from Equations 46, 48 and 50 that the real portion of the optical conductivity is related to the complex portion of the current-current correlation function

$$\sigma_1(\omega) = -\frac{1}{\omega} \text{Im} \chi(\omega), \quad (51)$$

where the current-current correlation function is given by

$$\chi(\omega) = \frac{1}{L} \sum_n |\langle 0 | j | n \rangle|^2 \left[\frac{1}{\hbar\omega - E_n + E_0 + is} - \frac{1}{\hbar\omega + E_n - E_0 + is} \right]. \quad (52)$$

The infinitesimal s arises from assuming that the perturbation in Equation 48 vanishes at $t = -\infty$. The states $|0\rangle$ and $|n\rangle$ are to be evaluated at $t = -\infty$ or $\mathbf{A} = 0$. The current operator in Equation 49 can be written in terms of the eigenstates of the system, following the same approach applied in Equations 32 through 38. The result is that

$$j_\nu = 4 \frac{teb}{L\hbar} \sum_{\mathbf{k}} \sum_{\lambda\lambda'} \left[u_{\mathbf{k}} (g\bar{Q}^\nu g) u_{\mathbf{k}}^\dagger \right]_{\lambda\lambda'} \sin(k_\nu b) \psi_{\lambda\mathbf{k}}^\dagger \psi_{\lambda'\mathbf{k}}. \quad (53)$$

Equation 53 is very similar to Equation 37. In this case, however, we are considering matrix elements connecting the ground state to excited states and so pick up the contributions at $\lambda \neq \lambda'$. Averaging the optical conductivity over the three directions in the lattice, it takes the form

$$\sigma_1(\omega) = \frac{\pi}{12|\chi|^2} \frac{e^2}{\hbar b} \left(\frac{t}{J} \right)^2 \frac{1}{\mu} \frac{1}{\mathcal{N}_m} \sum_{\mathbf{q}} F(\mathbf{q}) \delta(\mu - \Gamma_{\mathbf{q}}), \quad (54)$$

where $\Gamma_{\mathbf{q}}$ was defined in Equation 26 and where we have defined a dimensionless frequency given by $\mu = \hbar\omega/4J|\chi|$. The structure factor is given by:

$$F(\mathbf{q}) = \sum_{\nu} \sum_{\lambda=1}^2 \sum_{\lambda'=3}^4 \left| \left[u_{\mathbf{q}} (g\bar{Q}^\nu g) u_{\mathbf{q}}^\dagger \right]_{\lambda\lambda'} \right|^2 \sin^2 q_\nu b \quad (55)$$

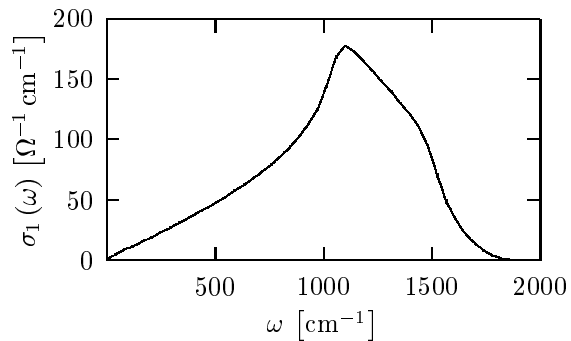


FIG. 6: Interband contribution to optical conductivity for the flux phase.

The sums in Equation 55 can be performed to give

$$F(\mathbf{q}) = \left(\frac{4}{3} + \frac{(\gamma_{\mathbf{k}} - \gamma_{\mathbf{k}}^*)^2}{6} \right) (\sin^2 k_x b + \sin^2 k_z b) + \frac{2}{3} (1 + \eta_{\mathbf{k}}^2) \sin^2 k_y b, \quad (56)$$

with the quantities defined as in Equation 26.

Equations 54 and 56 have been evaluated numerically, and the result is shown in Figure 6. Within our model, the location of the peak is proportional to the exchange energy J . Assuming this takes the value 0.1 eV, we find that the peak occurs at approximately 1000 cm^{-1} , which gives order of magnitude agreement with the observed value of 250 cm^{-1} in SrRuO_3 [1]. Due to the simplicity of the model we are solving, one would not expect more accurate agreement. The magnitude of the peak is governed by the ratio of t/J . Direct comparison of this quantity with experiment is more difficult. This is due to the fact that SrRuO_3 has five bands, whereas we have considered only a single orbital. Additionally, our calculation only considers the interband contribution to the conductivity, whereas the real material also has an intraband contribution from thermally excited carriers. If one assumes that the result shown in Figure 6 needs to be scaled by a factor of roughly five to account for the number of orbitals in SrRuO_3 , the results are reasonable compared with the measured conductivity of $6000 \text{ } \Omega^{-1} \text{ cm}^{-1}$.

VI. DISCUSSION

We propose that the three-dimensional flux state is a good candidate for the pseudogap state seen in the tran-

sition metal oxides. Its signature will be the presence of weak neutron diffraction peaks arising from the ordered electronic currents in the material. The fact that SrRuO_3 is not near an antiferromagnetic transition and the fact that the three dimensional flux states produce scattering at wavevectors other than $\mathbf{q}b = \boldsymbol{\pi}$ make the system an excellent candidate in which to observe this type of order. Further theoretical work is warranted to understand how the actual electronic structure of the material will influence the behaviors discussed here.

Acknowledgments

We would like to thank R. Krishna and J. Franklin for many useful discussions and S. Kivelson for inspirational remarks.

We acknowledge support from the DOE through the Complex Materials Program at SSRL.

APPENDIX

The matrices from Equations 22, 23, are given explicitly by

$$\begin{aligned} \alpha_x &= \begin{pmatrix} 0 & 0 & Ze^{-3i\pi/4} & 0 \\ 0 & 0 & 0 & Z^*e^{i\pi/4} \\ Z^*e^{3i\pi/4} & 0 & 0 & 0 \\ 0 & Ze^{-i\pi/4} & 0 & 0 \end{pmatrix} \\ \alpha_z &= \begin{pmatrix} 0 & 0 & Ze^{-i\pi/4} & 0 \\ 0 & 0 & 0 & Z^*e^{3i\pi/4} \\ Z^*e^{i\pi/4} & 0 & 0 & 0 \\ 0 & Ze^{-3i\pi/4} & 0 & 0 \end{pmatrix} \\ \alpha_y &= \begin{pmatrix} 0 & Z & 0 & 0 \\ Z^* & 0 & 0 & 0 \\ 0 & 0 & 0 & Z^* \\ 0 & 0 & Z & 0 \end{pmatrix}, \end{aligned} \quad (\text{A.1})$$

where

$$Z = e^{i\phi} = \frac{1}{\sqrt{3}} + i\sqrt{\frac{2}{3}}. \quad (\text{A.2})$$

-
- [1] P. Kostic, Y. Okada, N. C. Collins, Z. Schlesinger, J. W. Reiner, L. Klein, A. Kapitulnik, T. H. Geballe, and M. R. Beasley, *Phys. Rev. Lett.* **81**, 2498 (1998).
 [2] Y. S. Lee, J. S. Lee, K. W. Kim, T. W. Noh, J. Yu, E. J.

- Choi, G. Cao, and J. E. Crow, *Europhys. Lett.* **55**, 280 (2001).
 [3] L. Klein, J. S. Dodge, C. H. Ahn, J. W. Reiner, L. Mieville, T. H. Geballe, M. R. Beasley, and A. Ka-

- pitulnik, J. Phys.: Cond. Matt. **8**, 10111 (1996).
- [4] V. J. Emery and S. A. Kivelson, Phys. Rev. Lett. **74**, 3253 (1995).
 - [5] I. Affleck and J. B. Marston, Phys. Rev. B **37**, 3774 (1988).
 - [6] X. G. Wen, F. Wilczek, and A. Zee, Phys. Rev. B **39**, 11413 (1989).
 - [7] S. B. Libby, Z. Zou, and R. B. Laughlin, Nucl. Phys. B **348**, 693 (1991).
 - [8] A. Tikofsky, S. B. Libby, and R. B. Laughlin, Nucl. Phys. B **413**, 579 (1994).
 - [9] A. Zee, Int. J. Mod. Phys. B **5**, 529 (1991).
 - [10] I. I. Mazin, D. A. Papaconstantopoulos, and D. J. Singh, Physical Review B **61**, 5223 (2000).
 - [11] B. C. Chakoumakos, S. E. Nagler, S. T. Mixture, and H. M. Christen, Physica B **241–243**, 358 (1997).
 - [12] M. S. Laad and E. Müller-Hartmann, Phys. Rev. Lett. **87**, 246402 (2001).
 - [13] M. Inui, S. Doniach, and M. Gabay, Phys. Rev. B **38**, 6631 (1988).
 - [14] R. B. Laughlin and Z. Zou, Phys. Rev. B **41**, 664 (1989).
 - [15] T. C. Hsu, J. B. Marston, and I. Affleck, Phys. Rev. B **43**, 2866 (1991).
 - [16] E. Fawcett, Rev. Mod. Phys. **60**, 209 (1988).
 - [17] The reasoning leading to this result is identical to that of Affleck, Hsu and Marston for the two-dimensional flux states [15].